LEP Accelerator and Detectors

Reisaburo TANAKA
Department of Physics, Okayama University,
Tsushima-naka 3-1-1, Okayama 700-8530, Japan

The LEP experiment has finished in November 2000 after 12 years of operation. Highlights of the LEP accelerator and 4 LEP experiments, ALEPH, DELPHI, L3 and OPAL are reviewed.

1 Introduction

LEP was first conceived in 1976 by Burton Richter [1], after the November revolution in 1974, *i.e.* the discovery of J/Ψ particle at BNL and SLAC. A LEP-like machine at the centre-of-mass energy of 200 GeV was proposed to study the weak interactions. The LEP design and physics studies followed immediately after [2,3,4]. The LEP Summer Study in 1978 at Les Houces considered the physics issues in detail [5], Z^0 boson production and decay, $W^{\pm}$ pair production (to study the gauge cancellation), search for Higgs particle, search for new particles such as leptons and quarks and study of Quantum Chromo-Dynamics. It should be noted that W and Z weak gauge bosons were not discovered until 1983 at S$\bar{\text{p}}$pS by UA1 and UA2. The Les Houches summer study correctly foresaw the LEP physics programs which were actually carried out until 2000. The only missing issues were, a) missing energy measurement with hermetic detector (ex. SUSY was only very briefly mentioned) and b) B physics (it was not until the beginning of 1980's when the micro-vertex detectors were used at the collider detectors) .

In November 1982, six LoI's (Letter of Intent) for LEP experiment were submitted. The benchmark physics processes were 1) Z boson decay $Z \to b\bar{b}$ where B's are tagged with electron or muon, the measurement of forward-backward asymmetry $A_{FB}(b\bar{b})$, 2) B lifetime measurement, 3) neutrino counting by measuring the Z-width and via $\nu\nu\gamma$ process, 4) toponium search in $\zeta' \to \gamma +^3 P(t\bar{t}) \to \zeta + \gamma + \gamma(\zeta \to l^+l^-)$ or $\zeta' \to \gamma +^3 P(t\bar{t}) \to \gamma + hadrons$, 5) search for Higgs particle via Higgs-strahlung (Bjorken) process $e^+e^- \to Z + H$ and search for charged Higgs particle $e^+e^- \to H^+ + H^-$, and 6) search for free quarks of charge Q=1/3 and 2/3. Out of six LoI's, four experiments of ALEPH (spokesman: Jack Steinberger), DELPHI (Ugo Amaldi), L3 (Sam Ting) and OPAL (Aldo Michelini) were approved for construction. The other two proposals, ELECTRA and LOGIC were disapproved.

2 LEP Accelerator

The LEP design studies started at CERN in 1976 [1] and the first practical design was published in 1978 [3]. The proposed machine had a beam energy of 70 GeV with 22 km in circumference. In 1979, somewhat larger 30 km machine was proposed with emphasis on superconducting RF cavities, with which the beam energy could be brought above 100 GeV [4]. The final design

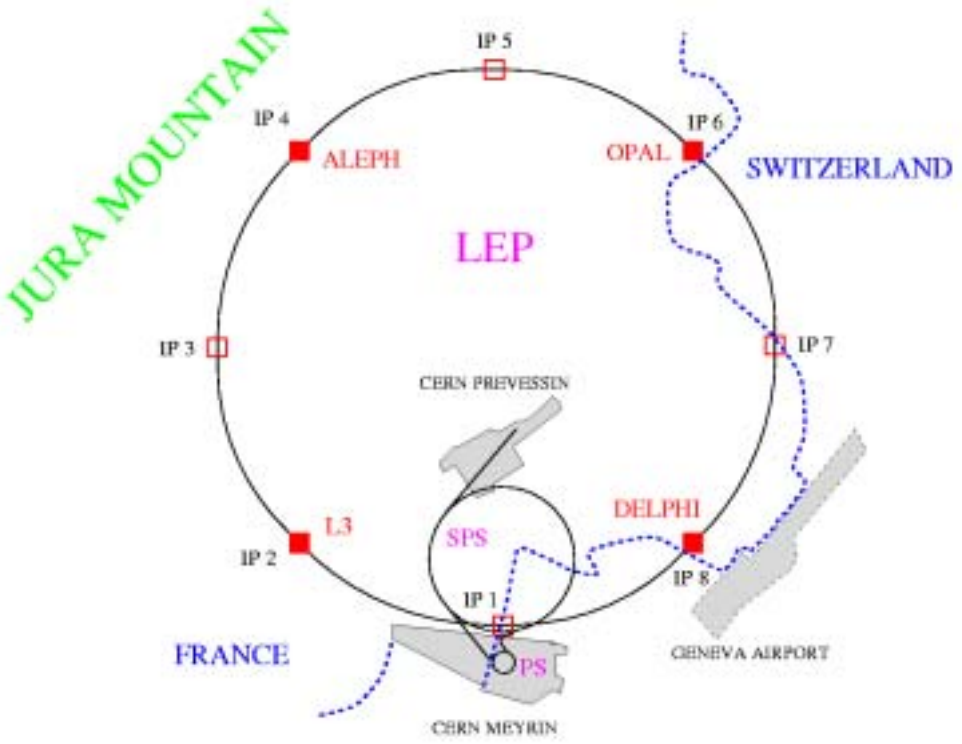

Figure 1: The layout of the LEP tunnel. The eight interaction points are denoted as IP1 through IP8. The four LEP experiments, ALEPH, DELPHI, L3 and OPAL were situated at the even number interaction points. Two LEP injectors, PS (Proton Synchrotron) and SPS (Super Proton Synchrotron) transported electrons (anti-clockwise) and positrons (clockwise) to the LEP ring.

featured the machine with a large circumference [6]. The LEP performance summary can be found in various reviews [7,8,9].

2.1 LEP Machine

Two fundamental parameters in the design of any collider are the beam energy and the luminosity. At LEP, the beam energy was defined to be able to study Z^0 and $W^{\pm}$ gauge boson properties, and resulted in a range of 40 to 200 GeV per beam.

The LEP ring extended from Jura mountain area to the Geneva airport, and 26.65 km in circumference as shown in Figure 1. There were eight collision points, from which 210 m straight section extended on both sides. There were eight 2.9 km arc sections. The LEP tunnel was 3.8 m in diameter and the depth varied between 50 and 175 m. About 3,400 dipole, 800 quadrupole, 500 sextupole and over 600 orbit correction magnets were installed in the tunnel. The magnet lattice was of FODO type with a period (cell) length of 79 m and 31 regular lattice periods per octant. The bending angle per period was 22.62 mrad.

The LEP commissioning started on the July 14, 1989 (the 200th anniversary of French revolution) when the first beam injected into the machine. By July 23, circulating beam had been established, and by August 4, a single beam had been taken to 45 GeV. LEP produced its first collision on August 13th, 1989, less than six years after the ground breaking on September 13th, 1983.

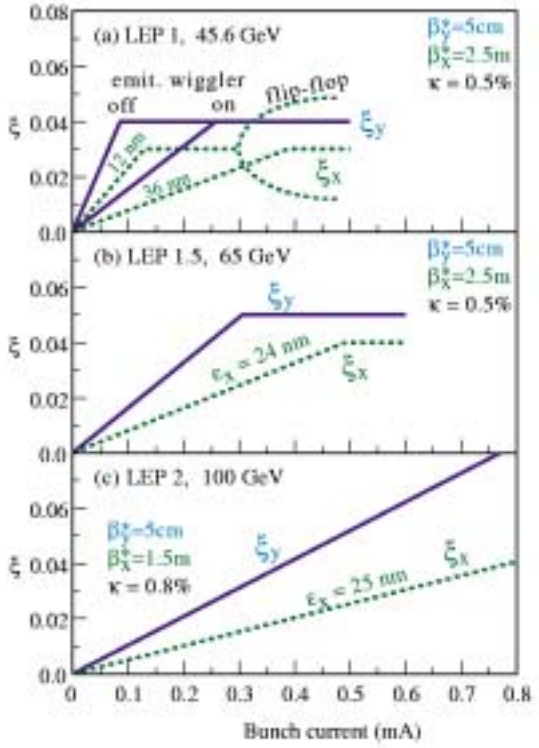

Figure 2: Schematic evolution of the beam-beam tune shifts ξ_x (dashed line) and ξ_y (solid line) with current at different LEP energies. At LEP2(c), the tune shift showed practically no sign of saturation.

2.2 RF Cavity

The crucial factor of the LEP design was the problem of synchrotron radiation wherein the transverse acceleration produced in circular accelerators leads to the emission of the electromagnetic radiation [10]. The amount of radiation is proportional to the fourth power of the beam energy and inversely proportional to the square of the bending radius in the dipole magnets. The energy lost must be resupplied by a Radio-Frequency (RF) system. In LEP at 100 GeV, the radiated power for a total intensity of 6 mA was about 18 MW. For beam energy of 104 GeV, about 3% of total energy was lost due to synchrotron radiation in one turn of the machine.

The RF acceleration system was installed in the straight sections around the four LEP experimental halls in the LEP tunnel. The first instance copper cavities were installed for 45.6 GeV beam operation at LEP1. The staged installation of superconducting RF cavities followed to enable the beam energy go beyond the W-pair production threshold at LEP2. In the final years of LEP operation, the RF system included 56 Cu-Cavity, 288 SC-Cavity (16 Nb and 272 Cu/Nb) together with 44 Klystrons The lengths of these cavities were 2.1 m for copper cavities and 1.7 m for super conducting cavities. The cavity gradient was achieved to be 7.5 MV/m after conditioning whereas the design value was 6.1 MV/m. A total accelerating voltage of 3,630 MV was provided to accelerate the beam up to 104 GeV [11,12,13,14].

2.3 Luminosity Optimization

One of the most important performance parameter at any collider is the luminosity which determines the number of events produced per unit time at each interaction region. A fundamental limitation to all electron-positron colliders results from the influence of the electromagnetic field associated with each beam on the motion of the particles in the other beam. In the case of

head-on collisions, this "beam-beam effect" is quantified by the beam-beam tune shift (ξ_y for vertical plane which is directly proportional to the luminosity).

LEP1

The original LEP design assumed that the electron and positron beams each consist of four equidistant bunches. These collided in the four interaction regions where an experiment was installed and were vertically separated by electrostatic separator bumps in the interleaved interaction points which were not equipped with an experiment. LEP was operated in this way from 1989 to 1992.

In the regime on the Z^0 resonance, the performance was constrained by the beam-beam effect which limited the bunch currents for collision. For low bunch currents, the beam sizes were not affected by the beam-beam forces. The horizontal (vertical) beam-beam tune shift ξ_x (ξ_y) increases linearly with beam current and the luminosity with the current squared. Above certain limit, the beam-beam interaction blew up the beam sizes and the beam-beam tune shift saturated at around 0.04 at LEP1 [15] as can be seen in Figure 2. As originally anticipated, the beam-beam interaction had been a stringent limit at the lower and intermediate beam energies.

The main breakthrough to increase the luminosity at LEP1 was an increase in the number of bunches, first with the Pretzel scheme commissioned in 1992 [16], and then with the bunch train scheme used in 1995 [17]. Both schemes reduced the bunch current that was collided and also the resultant beam-beam tune shift. However, the increase in number of bunches provided a net gain in luminosity.

- Pretzel scheme [16]

The idea for the Pretzel scheme originated at the Cornell's electron storage ring CESR, where the scheme has been used since 1983 [18]. In this scheme, the electrons and positrons travel on orbits which are distorted in opposite directions over practically the whole circumference of the machine by horizontal electrostatic fields. Parasitic beam-beam collisions can be arranged such that they occur where the separation between the two beams is almost maximum. Such a scheme has a potential for allowing a large number of bunches per beam. However, hardware and cost optimizations resulted in a scheme with eight equidistant bunches per beam at LEP. Pretzel scheme was used from 1992 through 1994.

- Bunch train [17]

The principle of the bunch train scheme is to string together individual bunches in trains wherein the distance between the bunches of a train is much smaller than the distance between the trains. In such a scheme, separation bumps are used to maximize the distance between bunches at potential parasitic encounters. The basic principle is illustrated in Figure 3 where the case of three bunches per train is shown. The bunch train scheme had been successfully used in LEP since 1995 with initially three and finally two bunches per train and four trains in each beam (up to twelve bunches per beam).

LEP2

After 1996, the beam energy was progressively increased from 80.5 GeV by installing more superconducting RF cavities and increasing the accelerating gradients. Above the $W^{\pm}$ threshold, the beam-beam limit was raised and an important beam-based challenge was to develop a low emittance optics with sufficient dynamic aperture to go to the 100 GeV regime. Luminosity was maximized by increasing the bunch current to the limit while operating with four bunches per beam and rigorous optimization of vertical and horizontal beam sizes.

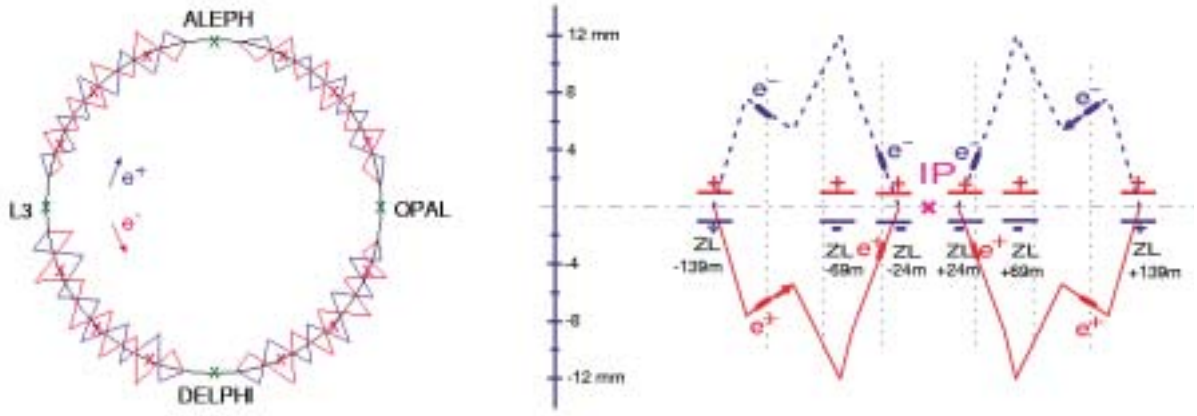

Figure 3: Schematic layouts of the Pretzel scheme (left) and Bunch Trains scheme (right) used at LEP. Pretzel scheme: the beams were separated horizontally in the mid-arcs to avoid unwanted collisions. Bunch Trains scheme: the beams were separated vertically around the eight interaction regions. The dotted vertical lines indicate the longitudinal position of parasitic encounters. Six electro static separators (ZL) were used to build the vertical separation bump.

2.4 LEP Performance

The performance at the beam energy of 45 GeV was very much constrained by the beam-beam effect which limited the bunch current that could be collided. The peak luminosities were well in excess of the design figure of 17×10^{30} cm^{-2}s^{-1} at LEP1.

The beam-beam limit was not reached for beam energies above 70 GeV. Higher bunch currents were allowed and optimization of the vertical beam size was possible. The record peak luminosity reached 10^{32} cm^{-2}s^{-1} and the vertical tune-shift parameter $\xi_y = 0.083$ per interaction point at the beam energy of 98 GeV. Above beam energy of 100 GeV, however, the luminosity decreased mainly due to lower beam currents, shorter fills and larger horizontal beam sizes.

The LEP operation is shown in Figure 4 and also summarized in Table 1 and 2, . It is notable that the continuous increase in luminosity was achieved at LEP1 phase thanks to efforts for multi-bunch scheme etc. The sizable increase in beam-beam tune shift when higher energies brought much higher luminosities at LEP2 phase. Increased instantaneous performance and operational efficiency as well as the evolution of the beam optics also contributed for best performances.

LEP delivered to each experiment an integrated luminosity over 200 pb^{-1} around Z^0 resonance and almost 800 pb^{-1} above the $W^{\pm}$ threshold. This corresponds to four million Z^0 bosons and around ten thousand $W^{\pm}$ boson pairs per experiment.

2.5 Beam Energy Calibration

LEP has provided the ideal place for the precise determination of the Z-boson mass and width at LEP1 as well as W-boson at LEP2. This required the precise determination of the centre-of-mass energy at the collision points. At LEP1, the beam energy was precisely calibrated by the resonant spin depolarization method. To extrapolate the beam energy calibrations over a long period of time, various effects causing energy changes had to be taken into account. Among these were the terrestrial tidal effect, surface motion due to rainfall and train effect as discussed below.

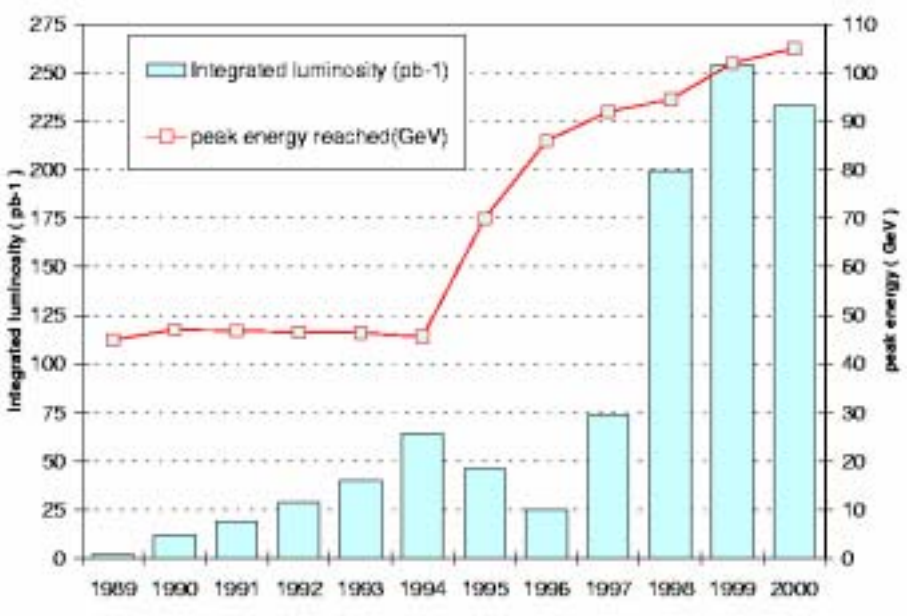

Figure 4: Summary of LEP operation. The maximum beam energies (plot) and the integrated luminosity per experiment for each year between 1989 and 2000 are shown.

Year	$\int \mathcal{L} dt$ (pb^{-1})	E_{beam} ($\mathrm{GeV/c^2}$)	κ_b	$2\kappa_b I_b$ (mA)	$\mathcal{L}$ ($10^{30}\ \mathrm{cm}^{-2}\ \mathrm{s}^{-1}$)	ξ_y
1989	1.74	45.6	4	2.6	4.3	0.017
1990	8.6	45.6	4	3.6	7	0.020
1991	18.9	45.6	4	3.7	10	0.027
1992	28.6	45.6	4/8	5.0	11.5	0.027
1993	40.0	45.6	8	5.5	19	0.040
1994	64.5	45.6	8	5.5	23.1	0.047
1995	46.1	45.6	8/12	8.4	34.1	0.030
1996	24.7	80.5-86	4	4.2	35.6	0.040
1997	73.4	90-92	4	5.2	47.0	0.055
1998	199.7	94.5	4	6.1	100	0.075
1999	253	98-101	4	6.2	100	0.083
2000	233.4	102-104	4	5.2	60	0.06

Table 1: Summary of LEP performance. The integrated luminosity, beam energy, number of bunches, total beam current, peak luminosity and maximum beam-beam tune shift parameter are shown.

Year	Optics	Comment	Bunch scheme
1989	60°/60°	LEP commissioned	4 on 4
1990	60°/60°		4 on 4
1991	60°/60°	90/90 tested	4 on 4
1992	90°/90°	Pretzel commissioned	4 on 4 / Pretzel
1993	90°/60°		Pretzel
1994	90°/60°		Pretzel
1995	90°/60°	Tests at 65-68 GeV	Bunch trains
1996	90°/60°	108/90 tested	4 on 4
1997	90°/60°	108/90 & 102/90 tests	4 on 4
1998	102°/90°		4 on 4
1999	102°/90°		4 on 4
	101.5°/45°	High-energy polarization optics	Single beam
2000	102°/90°	Max. energy 104.5 GeV	4 on 4

Table 2: Optics, main modes of operations and bunch scheme used at LEP1 and LEP2.

Transverse polarization

The lepton beams in LEP were self-polarized due to the Sokolov-Ternov effect [19]. The spin polarization builds up in the vertical transverse direction, and the maximum transverse polarization of 92.4% can be reached in an ideal storage ring. However, maximum polarization level is reduced in a real accelerator by resonances. The strong depolarization effect of the beam-beam force for large beam-beam tune shifts prevented the build-up of transverse polarization at LEP during normal physics runs.

Optimum polarization levels were achieved for beam energies corresponding to a spin tune close to a half-integer as shown in Figure 5. The highest polarization measured at LEP is also shown in the same figure. The record polarization level of 57 % was observed at LEP for beam energy of 44.72 GeV.

At higher energies, the maximum polarization level was reduced by the large energy spread and the strong synchrotron spin resonances. Polarization levels larger than 5 % were only observed up to 60.6 GeV. The vertical polarization was measured using Compton scattering of a circularly polarized laser beam.

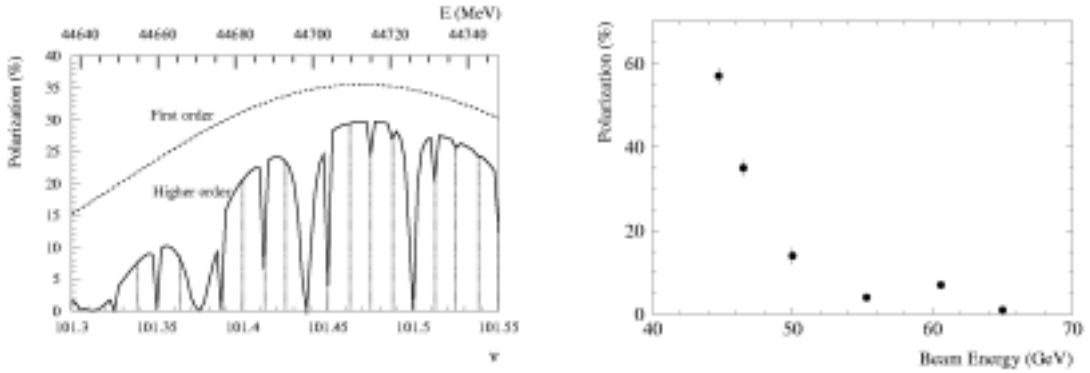

Figure 5: The transverse polarization expected from a first order and higher order calculations as a function of spin tune (left). Measured highest transverse polarization observed at LEP as a function of beam energy (right).

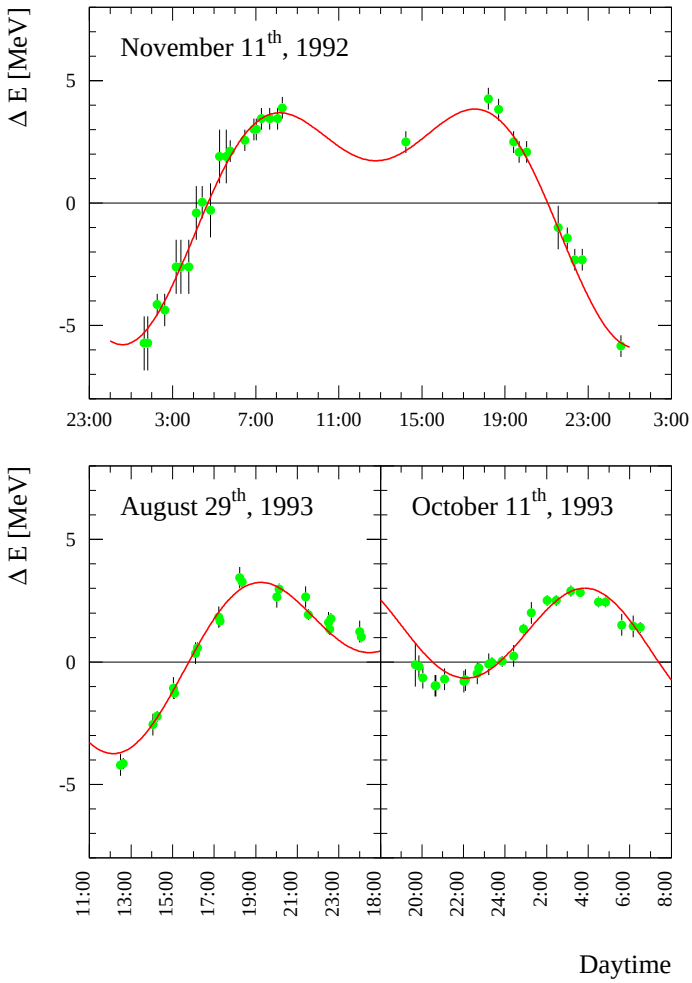

Figure 6: The evolution of the relative LEP beam energy variation due to tidal effect as a function of time. The solid lines are the predictions from the horizontal strain induced by the Earth tides. Top figure corresponds to full-moon, the bottom two figures to a time close to half-moon.

Resonant depolarization

Spin precession of a relativistic electron in electromagnetic fields is described by the Thomas-BMT equation [20]. In the storage ring, the spin vector of a particle precesses $a\gamma$ times for one revolution, where a is the term of anomalous magnetic moment of electron ($a = (g_e - 2)/2$) and $a\gamma$ is the spin tune.

The spin tune is directly proportional to the beam energy. The precise beam energy calibration by resonant depolarization of a polarized beam relies on this simple relation. If an external RF dipole field is applied in phase with the spin precession frequency, the spin vectors are resonantly rotated away from the vertical direction and the beam is depolarized. This method provided an extraordinarily high precision measurement. The average beam energy was determined with an absolute accuracy of about 0.2 MeV, or about 5×10^{-6} precision [21,22,23,24,25,26].

Circumference variations and tidal effect

Electrons and positrons circulating in the LEP ring were ultra-relativistic and traveled with almost light velocity. The length of their orbit was fixed by the RF frequency and the equilibrium beam energy had to adjust itself accordingly. The analysis of the LEP beam energy data suggested the previously unforeseen effect. The hypothesis of the tidal force was then raised.

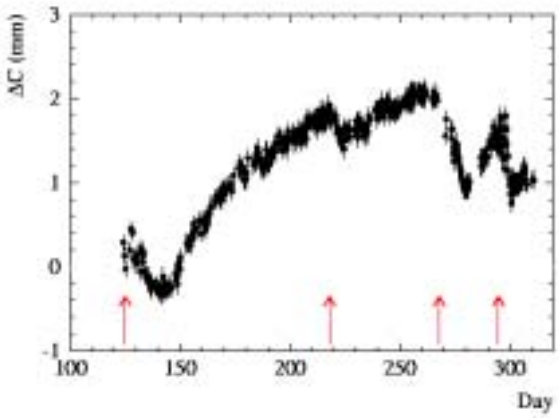

Figure 7: The evolution of the LEP circumference after the correction for tidal effect as a function of the day in 1999. After the heavy rainfall, indicated by the arrows, the circumference shrinked for some period before expanding again.

The gravitational attraction from the sun and moon is not uniform over the surface of the Earth because of the $1/r^2$ dependence of the gravitational forces. The terrestrial tides due to the sun and moon moves the Earth surface up and down. The lateral components of this motion modified the 26.7 km LEP circumference by about 1 mm. This change in length resulted in variations of the beam energy up to 120 ppm as can be seen in Figure 6. The observed variations agree well with the expectations from geophysical calculations. The measurement of the LEP beam energy clearly demonstrated that effect of the terrestrial tides on the LEP ring circumference and beam energy [27].

Besides the periodic tidal effect, the much slower long term effect was observed. Such effect was monitored by observing the radial movement of the beam relative to the quadrupoles in the beam position monitors. During a typical run lasting from May to November in each year, the LEP ring changed its circumference up to 2 mm as shown in Figure 7. This general trend was reproducible from one year to another. The circumference usually increased during summer season, and some of the changes were clearly correlated to the heavy rainfall which modified the underground water level. The monitoring of this seasonal change of the circumference turned out to be very important.

Magnetic field stability and TGV train

In 1995, a perturbation of the dipole field was observed when nuclear magnetic resonance (NMR) probes were installed in two tunnel dipoles to monitor the fields. As shown in Figure 8, the field fluctuation disappeared and remained stable between midnight and 4:30 am. The perturbation could be attributed to leakage currents flowing on the LEP vacuum chamber [28]. The currents were generated by trains circulating on a French railway line linking the cities of Geneva and Lyon which is operated at 1.5 kV DC. In contrast, Swiss railway lines are operated at 15 kV AC. For a given engine power, the DC currents were ten times higher and the leakage of DC current into the ground was large, with up to 25 % of the current not returning to the generator over the railway tracks. For LEP, the currents entered the tunnel around IP6 (OPAL) and exited the tunnel over the transfer lines to the SPS near IP1. The current itself did not induce energy changes because the net current averages to zero over the circumference. The correlation between railway currents LEP beam energy was clearly visible as shown in Figure 9.

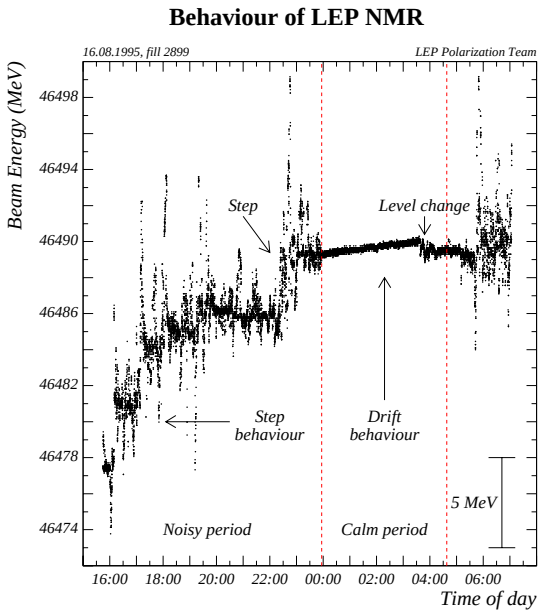

Figure 8: The LEP beam energy converted from NMR magnetic field measurement in a LEP dipole magnet over 10 hours.

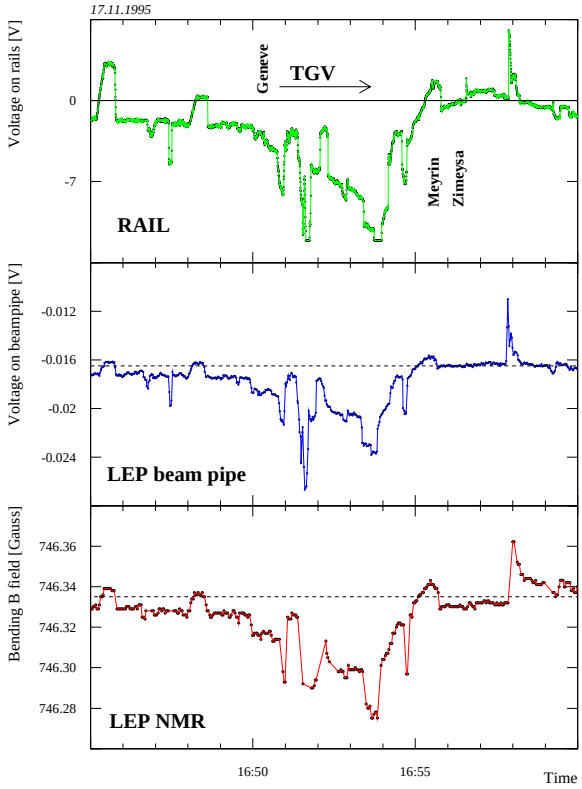

Figure 9: The voltage on rail of TGV train (top), voltage on LEP beam pipe (middle) and bending magnetic field measured by NMR at LEP (bottom).

Beam Energy

At LEP1, the resonant spin depolarization method provided the estimation of a systematic error due to the energy calibration of the LEP beams of only 1.7 MeV on Z-boson mass and of 1.3 MeV on Z-boson width [26]. This was far beyond the originally anticipated accuracy of Z-boson mass of about 20 MeV.

At LEP2, a direct energy calibration by resonant depolarization was not possible because transverse polarization was suppressed at such high energies as seen in Figure 5. The beam energy had to be extrapolated from measurements performed at lower energies between 41 and 61 GeV where sixteen NMR probes installed in LEP tunnel dipoles were cross-calibrated [29]. Calibration of the beam energy based on the relation between the synchrotron tune Q_s and the total accelerating voltage and based on the spectrometer beam position monitors were also studied to improve the precision on the estimation of the beam energy to be better than 20 MeV.

3 LEP Detectors

ALEPH

The ALEPH detector [30] was a 4π detector designed to give as much detailed information as possible about complex events in high-energy e^+e^- collisions.

A superconducting coil, 5 m in diameter and 6 m long, produced a uniform 1.5 Tesla field in the beam direction. Inside the coil, in order of increasing radius, there were a microstrip solid state device, an Inner Tracking Chamber (ITC) using drift wires, a Time Projection Chamber (TPC), 3.6 m diameter, 4.4 m long, and an electromagnetic calorimeter of 2 mm lead sheets with proportional wire sampling. Outside of the coil, a 1.2 m thick Fe return path was used as a hadron calorimeter, and a double layer of drift tubes aided in the muon identification.

Strong points of the detector were a precision of momentum measurements for charged particles, due to a high magnetic field and a TPC, a good identification of electrons and muons even when they were immersed in jets, and a spatial resolution obtained in e-γ calorimetry. A minivertex detector provided a capability for identifying secondary vertices, and a silicon-tungsten calorimeter installed in 1992 allowed a significant reduction of the luminosity error.

DELPHI

The DELPHI detector [31] was a general purpose detector offering 3-dimensional information on curvature and energy deposition with fine spatial granularity, as well as identification of leptons and hadrons over most of the solid angle.

A superconducting coil provided a 1.2 Tesla solenoidal field of high uniformity. Tracking relied on a micro-vertex detector, an inner detector, TPC, an outer detector, and forward drift chambers. A 3-layer silicon microvertex detector allowed a precision measurement of the interaction vertex and decay vertices of short-lived particles such as bottom and charm hadrons and tau leptons.

Electromagnetic showers were measured in the barrel with high granularity by the High Density Projection Chamber (HPC) and in the endcaps by 1×1 degree projective towers composed of lead glass as an active material and phototriode readout. Hadron identification was provided mainly by liquid and gas Ring-Imaging Čerenkov counters (RICH). A segmented magnet yoke served for hadron calorimetry and as a filter for muons which were identified in two drift chamber layers. In addition, scintillator systems were implemented in the barrel and forward regions. A small angle Shashlik-type calorimeter (STIC) was used for the luminosity determination.

L3

The L3 detector [32] consisted of a high-volume low-field solenoid magnet, a small central tracking chamber with very high spatial resolution, a high-resolution electromagnetic calorimeter encapsulating the central detector, a hadron calorimeter acting also as a muon filter, and high-precision muon tracking chambers.

The detector was designed to measure energy and position of leptons with the highest obtainable precision allowing a mass resolution $\Delta M/M$ smaller than 2 % in dilepton final states. Hadronic energy flux was detected by a fine-grained calorimeter, which also served as a muon filter and a tracking device.

The outer boundary of the detector was given by the iron return-yoke of a conventional magnet. The field was 0.5 Tesla over a length of 12 m. The muon momentum measurement was performed by three sets of drift chambers in the central detector region. A forward-backward muon detection system extended the polar angle coverage to 22 degrees in the forward region.

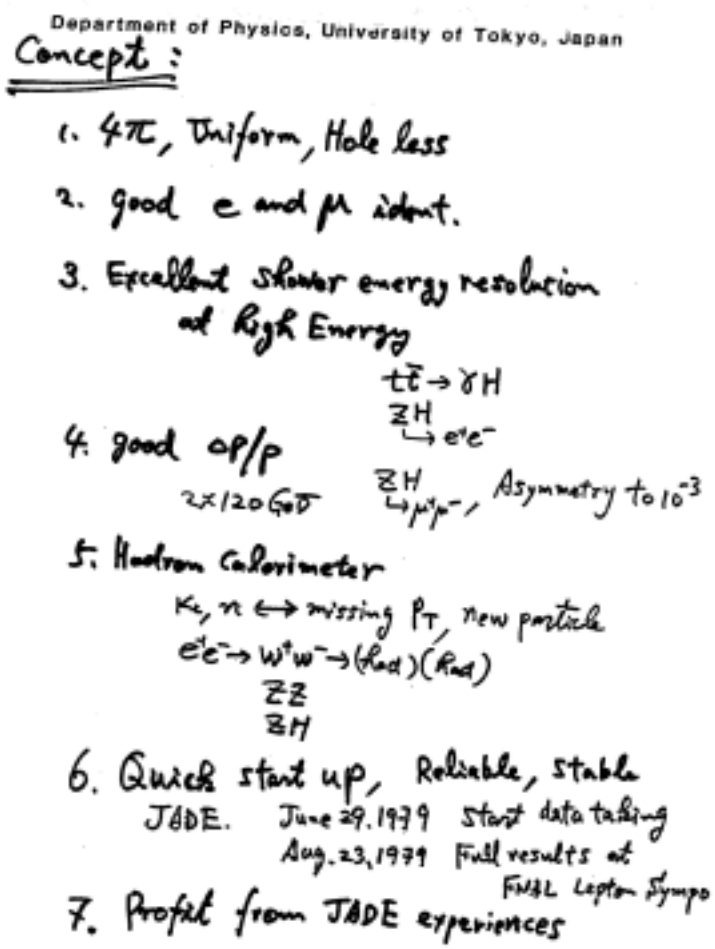

Figure 10: The OPAL detector concept by Professor S. Orito.

Radially inwards were a combined hadron calorimeter and muon absorber. The electromagnetic energy flow was determined by approximately 11,000 crystals of BGO. Full electromagnetic shower containment over nearly 4π solid angle coverage was achieved. Surrounding the 10 cm diameter beam pipe, a high-precision Silicon Microstrip Detector (SMD) and a small drift chamber operating in the time expansion mode (TEC) acted as charged particle vertex detectors.

OPAL

The general purpose detector OPAL[33] was designed to study a wide range of unexplored physics at LEP. The main components of the apparatus, in order of increasing distance from the interaction point, were a silicon micro-vertex detector, central detectors consisting of a vertex and a jet chamber, and a barrel of Z chambers, a warm conductor solenoid providing a uniform magnetic field of 0.4 Tesla, a TOF scintillator barrel detector, complimented by a scintillating tile endcap detector, a 4π lead glass electromagnetic calorimeter, a hadron calorimeter instrumented by streamer tubes and thin gap wire chambers, an external muon identifier, and a forward detector which included a new small-angle silicon-tungsten calorimeter.

Figure 10 displays the sketch of the concept for OPAL detector by Professor S. Orito[34].

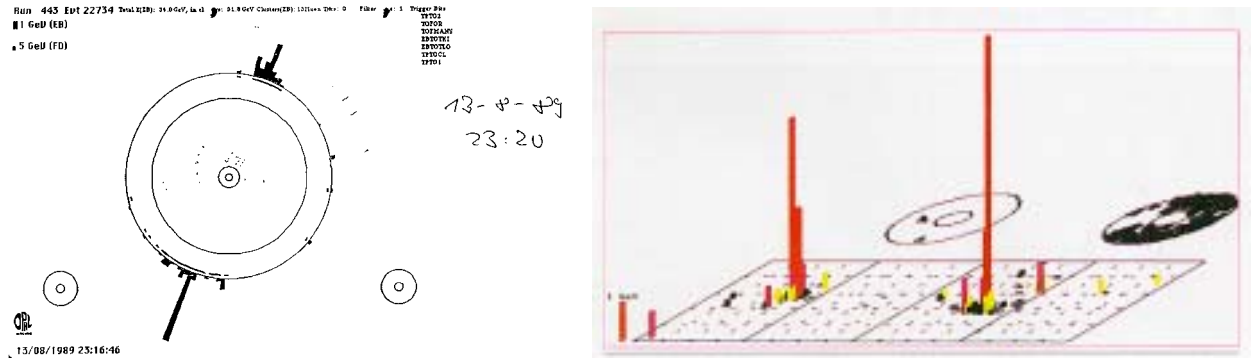

Figure 11: The first Z event observed by OPAL in $r-\phi$ view (left) and lego plot (right). The two hadronic jets were observed in the calorimeter. At the moment, the tracking chambers were not yet fully operational and no particle tracks were seen in the central detector.

Among the central physics issues were the study of the Z^0 and $W^{\pm}$ gauge bosons. A general search for new particles, in particular the Higgs bosons, was mentioned as well as the importance of missing P_T measurement. The importance of the quick start-up with reliable and stable detector was stressed profiting the experience from JADE experiment at PETRA. Among four LEP experiments, OPAL, indeed, observed the first Z event on August 13, 1989 as displayed in Figure 11.

3.1 Central Tracker

LEP environment provided the ideal experimental conditions for tracking. The event rate was of the order of 1 Hz with long time between two beam-crossings. There were very low machine backgrounds, and the trigger mostly collected all events with detector dead time nearly equal to zero. Tracks were distributed over the full solid angle with very little weight of forward/backward cones. The clustering of tracks was only due to the jet structure. Thus full reconstruction for each event was possible at LEP.

Table 3 summarizes the design concept of the central trackers. Among those, the original idea of the Time Projection Chamber (TPC) goes back to G. Charpak in 1970 when he designed the chamber with long drift distances. The pioneering works were carried out by D. Nygren in 1970's which fruited to the construction and operation of the TPC at PEP-4 [35] . The decision to use the TPC was hard for ALEPH and DELPHI, and both needed big prototypes equipped with laser beams. In ALEPH, the TPC was considered as a risky option, but the prototype exhibited the clear success, and it was the jewel of ALEPH in the end.

The performances of central trackers are summarized in Table 4. These large central tracking chambers demonstrated the superb pattern reconstruction capability in truly three dimensional (TPC) with particle separation of the order of 2 mm in space. Also very good momentum

	Wire Chamber	TPC
Small or Medium size	L3 - TEC B = 0.5 T 2 Atm.	DELPHI - TPC B = 1.2 T 1 Atm.
Large size	OPAL - JET B = 0.43 T 4 Atm.	ALEPH - TPC B = 1.5 T 1 Atm.

Table 3: Summary of the design concept of the central trackers for LEP experiments.

	ALEPH	DELPHI	L3	OPAL
Length [cm]	440	260	120	400
Outer radius [cm]	170	110	48	185
Inner radius [cm]	33	40	11	25
Pressure [Atm.]	1	1	2	4
B [Tesla]	1.5	1.2	0.5	0.435
Points/Track	21 pads	16 pads	62 wires	159 wires
dE/dx samples	340	192	-	159
$\sigma_{r\phi}$ [μm]	170	250	50	135
σ_z [mm]	1	1	20 (C.D.)	60 (C.D.)
σ/p [GeV/c]$^{-1}$	1.2×10^{-3}	$5 - 7 \times 10^{-3}$	10×10^{-3}	1.5×10^{-3}
Particle ID				
π/e (3σ)	$\leq$8 GeV/c	$\leq$8 GeV/c	-	$\leq$8 GeV/c
π/K (2σ)	$\leq$17 GeV/c	$\leq$30 GeV/c	-	$\leq$20 GeV/c

Table 4: Summary of the geometry and operational performances of the central trackers for LEP experiments.

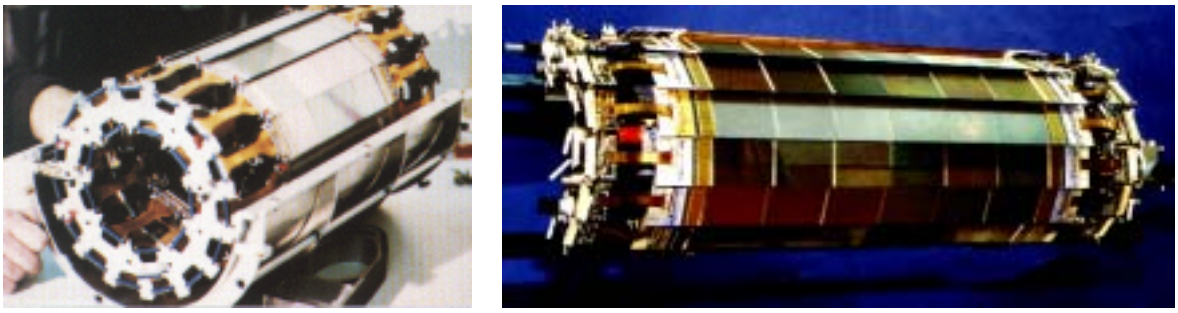

Figure 12: The ALEPH vertex detectors for LEP-1 (left) and LEP-2(right).

resolution of $\sigma_p \simeq 10^{-3}p$ [GeV/c] was obtained with capability of particle identification via dE/dx.

3.2 Vertex Detector

In 1960's, silicon detectors were used for nuclear physics. After the discovery of charm quark in 1974, the measurement of the lifetime of D-mesons were carried out using the silicon as active target. Then the idea to subdivide one electrode into thin strips emerged in 1980's. The main problem was the packaging of the electronics, but the development of microelectronics enabled the micro-vertex detector to become reality. The first design of a silicon vertex detector was given in 1981 for collider detectors ALEPH at LEP and CDF at Tevatron. This opened the door to the heavy flavour physics of top, bottom, charm and tau as well as Higgs.

For LEP1, the first generation detectors consisted of single or double sided 2-layers. For LEP2, longer detectors were designed to enable the larger acceptance with double sided 2 or 3 layer as shown in Figure 12. The mechanical design and the performances are summarized in Table 5 [36].

The silicon vertex detector played the key role of τ and B-physics at LEP. A nice event of $B^0 \to J/\psi K^0_S$ with $J/\psi \to e^+e^-$ observed by ALEPH [37] is displayed in Figure 13.

	ALEPH	DELPHI	L3	OPAL
Layers	2	3	2	2
Radii [cm]	6.3, 11.0	6.6, 9.2, 10.6	6.4, 7.9	6.1, 7.4
Modules/layer	9, 15	24, 20, 24	12	12, 15
Sensors/module	6	4, 8	4	5
Module length [cm]	40	28, 48	28	30
Max $\lvert\cos\theta\rvert$	0.88, 0.95	0.91, 0.93	0.83, 0.93	0.89, 0.93
Channels	95,000	150,000	73,000	65,000
Front-end chip	MX7-RH	MX6, TRIPLEX	SVX-H3	MX7, MX7-RH
Sensor-type	double-sided	double + single	double-sided	single-sided
Readout pitch [μm]				
ϕ	50	50	50	50
z	100	44 - 176	150, 200	100
Cooling	Water + Air	Water	Water	Water + Nitrogen
Sensitive area [m^2]	0.96	1.37 + 0.41(VFT)	0.52	0.53
$r-\phi$ plane				
S/N	31	10-28	18	24/29
Impact param.				
resol. [μm]	34[a]	25	30	18
Point resolution [μm]	10	8	8	8-10
z				
S/N	18	10-28	18	20/24
Impact param.				
resol. [μm]	34[a]	34	130	24
Point resolution [μm]	15	11	20	10-12
Multiple scatt.				
term[b]. [μm GeV/c]	70	70	80	100

Table 5: Characteristics and performance figures of the silicon vertex detectors at LEP2. [a]ALEPH quotes the resolution for a three dimensional impact parameter. [b]Estimated from fits with one constant term and one proportional to $1/(P\sin^{3/2}\theta)$, where P is the momentum and θ the polar angle.

	ALEPH	DELPHI	L3	OPAL
ECAL				
barrel	Pb/wires	Pb/drift	BGO	Lead Glass
granularity [μsr]	13 × 13	15 × 6	34 × 34	40 × 40
longitudinal	3	9	1	1
segmentation	45 planes			presampler
σ_E at 46 GeV	3.5 %	6.5 %	1.5 %	2.5 %
endcap	Pb/wires	Lead Glass	BGO	Lead Glass
HCAL				
barrel	Fe/streamers	Fe/streamers	U/wires	Fe/streamers
granularity [μsr]	52 × 52	50 × 75	42 × 42	120 × 120
longitudinal	1/10 planes	4	10	1
segmentation				
σ_E at 46 GeV	100 %	112 %	55 %	120 %
endcap	Fe/streamers	Fe/streamers	U/wires	Fe/streamers
Luminometer	Si/W	Shashlik	BGO	Si/W

Table 6: Characteristics and performance figures of the electromagnetic (ECAL), hadronic (HCAL) and luminosity calorimeters.

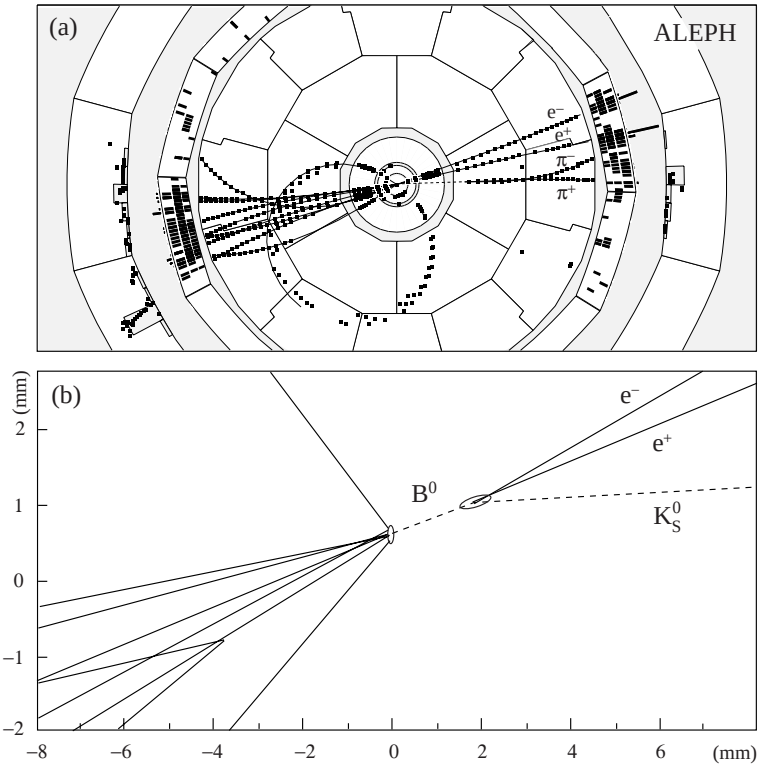

Figure 13: The gold-plated CP-violating event $B^0 \to J/\psi K_S^0$ with $J/\psi \to e^+e^-$ seen by ALEPH: (a) view of the projection transverse to the beam axis, (b) zoom on the vertex region, with reconstructed vertices marked with ellipses (neutral particles are marked with dashed lines).

3.3 Calorimeter

Calorimetry at LEP provided the four functions, trigger, measurement, identification and veto[38]. The calorimeter measured the energies of γ's and neutral hadrons as well as electrons which can be better measured by calorimetry than by tracking. It also provided the measurements on charged hadrons. The identification of γ's and π^0's, neutral hadrons, muons and electrons, charged hadrons was carried out to measure the energy flow.

The general characteristics of electromagnetic, hadronic and luminosity calorimeters are summarized in Table 6. For barrel electromagnetic calorimeter (ECAL), ALEPH and DELPHI chose the sampling type, whereas L3 and OPAL used the homogeneous (crystal) type. The OPAL barrel ECAL of 9,440 channels as shown in Figure 14 was operated with all channels alive over the LEP's 12 years. Congratulations for ICEPP, University of Tokyo group for this great success!

3.4 Energy Flow

For jets which originate from hadronic decay of Z^0 and $W^\pm$ gauge-bosons or Higgs boson, it is essential to assess the energy deposited in the detector and its direction, the energy flow. Tracking can be used for all the charged tracks, and the sole neutrals are measured by the calorimeters. The energy flow can be defined as:

$$E_{tot} = p_e + p_\mu + p_{\text{charged hadron}} + E_\gamma + E_{\text{neutral hadon}}$$

where momentum of electrons, muons and charged hadrons are measured by trackers, whereas energies of γ's and neutral hadrons are measured with calorimeters. To improve the energy flow resolution, the capability to identify neutral particles such as γ's and π^0's, neutron, K_L^0 are

Figure 14: Fish-eye view of the OPAL barrel Lead-Glass electromagnetic calorimeter.

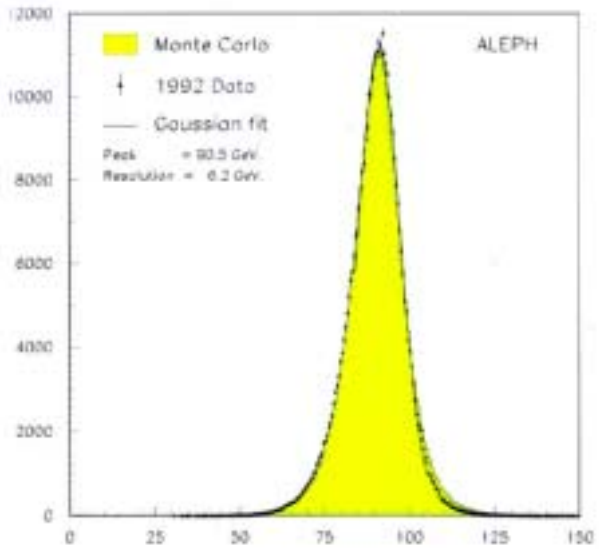

Figure 15: The enegy flow of Z bosons from well-contained hadronic events seen by the ALEPH detector. Plots are data taken in 1992, and the histogram shows the Monte Carlo simulation.

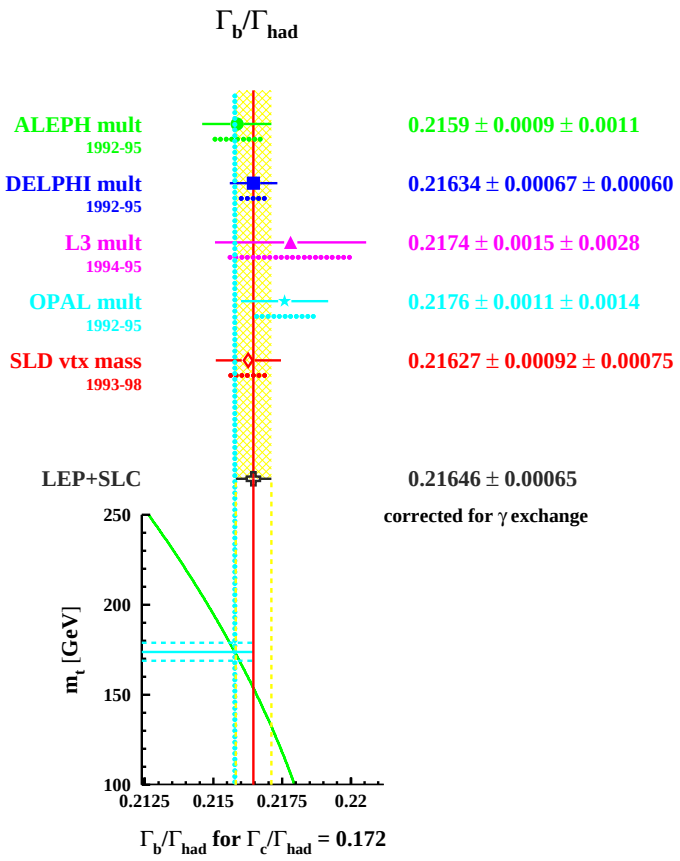

Figure 16: Summary of measurements of $R_b = \Gamma_b/\Gamma_{had}$ by LEP and SLD experiments. Prediction as a function of top quark mass is shown in the bottom.

most important, This lead to the design of fine granular and hermetic calorimeter as aimed by ALEPH. Generally, the calorimetric response to electrons and pions are not the same. The e/π ratio can, however, be corrected to unity via software correction as done in ALEPH.

This energy flow performance by the ALEPH detector[30] is shown in Figure 15. The energy-flow resolution is $\sigma_{\text{Energy Flow}} = 0.59\sqrt{E(\text{GeV})}$. Traditionally, the energy-flow had been taken as $E_{\text{tot}} = E_{\text{ECAL}} + E_{\text{HCAL}}$, where E_{ECAL} and E_{HCAL} correspond to electromagnetic and hadronic energies, respectively. This classical energy-flow only provided the resolution of $1.2\sqrt{E(\text{GeV})}$. The improvement with high quality LEP tracking and with high granularity of calorimeters is evident.

3.5 Impact on Physics Performance

The importance of the silicon vertex detector can be seen in Figure 16 where the $R_b = \Gamma_b/\Gamma_{had}$ is shown for LEP and SLD experiments. Since DELPHI had 3-layers of silicon while others had 2-layers, better measurement on R_b had been carried out. Also very precise results was obtained by SLD collaboration using the charge-coupled device (CCD) vertex detector with 3.07×10^8 pixels[39]. The vertex detector was at inner radius of 2.7 cm with three layer system. The track impact parameter resolution was $7.7 \times 9.6\mu$m in $(r\phi, z)$ plane.

The importance of fine granular calorimeter is demonstrated in Figure 17. The vector and axial-vector neutral current couplings of g_V and g_A determines $A_f = 2g_V \cdot g_A/(g_V^2 + g_A^2)$. A_τ and A_e measured from tau polarization are shown. ALEPH has performed the measurement nearly

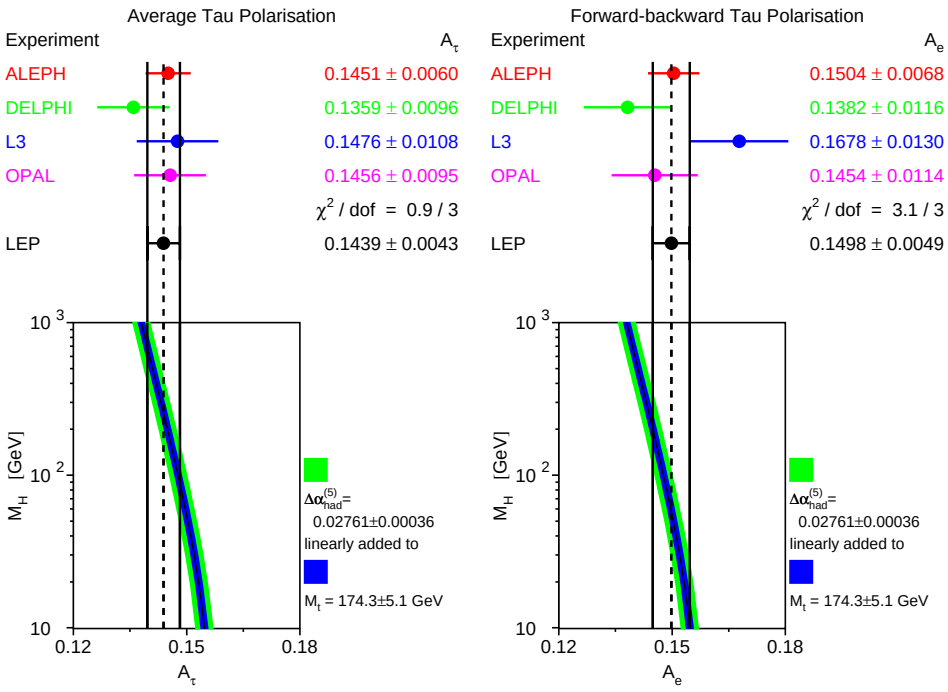

Figure 17: Summary of A_τ (left) and A_e (right) measurements from tau polarization.

twice better than any other experiments. This was due to better capability of neutral particle identification such as γ's and π^0's as well as charged particles.

4 Summary

At the design phase of the LEP experiment in 1970's, the physics programs such as electroweak physics with Z^0 and $W^\pm$ gauge bosons, search for new particles including Higgs particle and QCD were correctly foreseen. The only exceptions were missing energy measurement with hermetic detector to search for SUSY particles and B physics using the silicon micro-vertex detector. The importance of these subjects only emerged in the beginning of 1980's.

LEP was successfully operated from 1989 to 2000 over 12 years [40]. LEP had never been the same accelerator each year. Six optics were in operation with 2×2 to 16×16 bunches. Wide beam energy range was covered from 45 to 104.5 GeV. About 4,000 physics fills were accumulated and LEP provided the total integrated luminosity of 1 fb^{-1} for each experiment, which enabled the unprecedented high precision test of the Standard Model. A highly dedicated machine group was responsible for the excellent performance of LEP.

Concerning the detector, LEP was the pioneer for new generation of particle detectors. Most important was the silicon micoro-vertex detector which emerged in the beginning of 1980's. High precision vertex tag opened the new era of heavy flavour physics of top, bottom, charm and tau. It also played the key role for the search for Higgs particle. The time projection chamber enabled the fully three-dimensional tracking. The importance of fine granular hermetic calorimeter was recognized for various physics performances including the energy-flow measurement for jet physics. These trends will continue at forthcoming LHC and Linear Collider experiments.

References

1. B. Richter, *"Very High-Energy Electron-Positron Colliding Beams for the Study of the Weak Interactions"*, *Nucl. Instrum. Methods* **136** (1976) 47.
2. L. Camilleri *et al.*, *"Physics with Very High-Energy e^+e^- Colliding Beams"*, CERN Yellow Report, CERN-76-18, 1976.
3. The LEP Study Group, *"Design Study of a 15 to 100 GeV e^+e^- Colliding Beam Machine (LEP)"*, CERN Report ISR-LEP/78-17, 1978.
4. The LEP Study Group, *"Design Study of a 22 to 130 GeV e^+e^- Colliding Beam Machine (LEP)"*, CERN Report ISR-LEP/79-33, 1979.
5. *"LEP Summer Study, Les Houches and Geneva"*, CERN Yellow Report, CERN-79-01, 1979.
6. *"The LEP Injector Chain"*, The LEP Design Report Vol.I, CERN Report LEP/TH/83-29, 1983,
   "The LEP Main Ring", The LEP Design Report Vol.II, CERN Report LEP/TH/84-01, 1984,
   "LEP2", The LEP Design Report Vol.III, CERN Report AC/96-01, 1996.
7. D. Brandt *et al.*, *"Accelerator Physics at LEP"*, *Rep. Prog. Phys.* **63** (2000) 939.
8. R. Assmann, M. Lamont and S. Myers, *"A Brief History of the LEP Collider"*, CERN Report CERN-SL-2002-009 OP, 2002.
9. G. Arduini *et al.*, *"LEP1 Operation, 1989-1995"*, CERN Report CERN-SL-96-43 OP, 1996.
10. M. Sands, *"The Physics of Electron Storage Rings: An Introduction"*, SLAC Report SLAC-R-121, 1970, *http://www.slac.stanford.edu/pubs/slacreports/slac-r-121.html* .
11. P. Brown *et al.*, *"Performance of the LEP200 Superconducting RF System"*, CERN Report CERN-SL-99-075 LRF, 1999.
12. P. Brown *et al.*, *"Ultimate Performance of the LEP RF System"*, CERN Report CERN-SL-2001-018 HRF, 2001.
13. K. Hübner , *"The LEP Superconducting RF System"*, CERN Report CERN-SL-2001-059 DI, 2001.
14. P. Brown *et al.*, *"Operating Experience with the LEP200 Superconducting RF System"*, CERN Report CERN-SL-2002-004 HRF, 2002.
15. H. Burkhardt *et al.*, *"The Effect of the Beam-Beam Interaction on the Performance of LEP"*, CERN Report CERN-SL-92-15 DI, 1992.
16. J. M. Jowett, W. Kalbreier and S. Mayers, *"Preparations for High-Luminosity LEP"*, in Proceedings of the 2nd European Particle Accelerator Conference, Nice, France, 12-16 Jun 1990, p.403-405.
17. B. Goddard *et al.*, *"Bunch Trains for LEP"*, *Part. Accel.* **57** (1997) 237.
18. R. M. Littauer, *"Multibunch Operation of CESR"*, *IEEE Trans. Nucl. Sci.* **32** (1985) 1610.
19. A. A. Sokolov and I. M. Ternov, *"On Polarization and Spin Effects in the Theory of Synchrotron Radiation"*, *Sov. Phys. Dokl.* **8** (1964) 1203.
20. V. Bargmann, L. Michel and V. L. Telegdi, *"Precession of the Polarization of Particles Moving in a Homogeneous Electromagnetic Field"*, *Phys. Rev. Lett.* **2** (1959) 435.
21. L. Arnaudon *et al.*, *"The Energy Calibration of LEP in 1991"*, CERN Preprint CERN-PPE-92-125, CERN-SL-92-37 DI, 1992.
22. L. Arnaudon *et al.*, *"Measurement of LEP Beam Energy by Resonant Spin Depolarization"*, *Phys. Lett.* B **284** (1992) 431.
23. L. Arnaudon *et al.*, *"Measurement of the Mass of the Z Boson and the Energy Calibration of LEP"*, *Phys. Lett.* B **307** (1993) 187.
24. R. Assmann *et al.*, *"The Energy Calibration of LEP in the 1993 Scan"*, *Z. Phys.* C **66**

(1995) 567.
25. L. Arnaudon *et al.*, *"Accurate Determination of the LEP Beam Energy by Resonant Depolarization"*, *Z. Phys.* C **66** (1995) 45.
26. R. Assmann *et al.*, *"Calibration of Center-of-Mass Energies at LEP-1 for Precise Measurements of Z Properties"*, *Eur. Phys. J.* C **6** (1999) 187.
27. L. Arnaudon *et al.*, *"Effects of Terrestrial Tides on the LEP Beam Energy"*, *Nucl. Instrum. Methods* A **357** (1995) 249.
28. E. Bravin *et al.*, *"The Influence of Train Leakage Currents on the LEP Dipole Field"*, *Nucl. Instrum. Methods* A **417** (1998) 9.
29. A. Blondel *et al.*, *"Evaluation of the LEP Center-of-Mass Energy above the W Pair Production Threshold"*, *Eur. Phys. J.* C **11** (1999) 573, *ibid.* **11** (1999) 729.
30. D. Decamp *et al.*, ALEPH Collaboration, *"ALEPH: A Detector for Electron-Positron Annihilations at LEP"*, *Nucl. Instrum. Methods* A **294** (1990) 121, Erratum *ibid.* **303** (1991) 393;
D. Buskulic *et al.*, *"Performance of the ALEPH Detector at LEP"*, *Nucl. Instrum. Methods* A **360** (1995) 481.
31. P. A. Aarnio *et al.*, DELPHI Collaboration, *"The DELPHI Detector at LEP"*, *Nucl. Instrum. Methods* A **303** (1991) 233; P. Abreu *et al.*, *"Performance of the DELPHI Detector"*, *Nucl. Instrum. Methods* A **378** (1996) 57, Erratum *ibid.* **396** (1997) 281.
32. B. Adeva *et al.*, L3 Collaboration, *"The Construction of the L3 Experiment"*, *Nucl. Instrum. Methods* A **289** (1990) 35; O. Adriani *et al.*, *"Results from the L3 Experiment at LEP"*, *Phys. Rept.* **236** (1993) 1.
33. K. Ahmet *et al.*, *"The OPAL Detector at LEP"*, *Nucl. Instrum. Methods* A **305** (1991) 275.
34. S. Orito, *"OPAL Detector at LEP"*, in Proceedings of New Detectors For High Energy Physics, Tsukuba, Japan, 1982, p.1-13.
35. D. R. Nygren, *"Future Prospects of the TPC Idea"*, *Phys. Scripta.* **23** (1981) 584.
36. J. M. Heuser, *"Experience with the Construction, Operation and Maintenance of Vertex Detectors at LEP"*, *Nucl. Instrum. Methods* A **418** (1998) 1; K. Österberg, *"Performance of the Vertex Detectors at LEP2"*, *Nucl. Instrum. Methods* A **435** (1999) 1.
37. R. Barate *et al.*, ALEPH Collaboration, *"Study of the CP Asymmetry of $B^0 \to J/\psi K^0_S$ Decays in ALEPH"*, *Phys. Lett.* B **492** (2000) 259.
38. H. Videau, *"ALEPH Choices on Calorimetry in the Light of LEP Physics"*, in Proceedings of the 2nd International Conference on Calorimetry in High-energy Physics, Capri, Italy, Oct. 14-18, 1991, Eds. A. Ereditato *et al.*, World Scientific, p.454-459;
"Calorimetry at LEP, a Critical Point of View", in Proceedings of the 6th International Conference on Calorimetry in High-Energy Physics (ICCHEP'96), Jun. 8-14, 1996, Rome, Italy, Eds. A. Antonelli *et al.*, Frascati Physics Series; 6, p.905-916.
39. K. Abe *et al.*, *"Design and Performance of the SLD Vertex Detector, a 307 Mpixel Tracking System" Nucl. Instrum. Methods* A **400** (1997) 287.
40. LEP Fest 2000, Oct. 9-11, 2000, CERN,
http://cern.web.cern.ch/CERN/Announcements/2000/LEPFest/ .